

---

Dear Author,

**Please correct your galley proofs carefully and return them no more than four days after the page proofs have been received.**

**Please limit corrections to errors already in the text; cost incurred for any further changes or additions will be charged to the author, unless such changes have been agreed upon by the editor.**

The editors reserve the right to publish your article without your corrections if the proofs do not arrive in time.

Note that the author is liable for damages arising from incorrect statements, including misprints.

Please note any queries that require your attention. These are indicated with a Q in the PDF and a question at the end of the document.

**Reprints** may be ordered by filling out the accompanying form.

Return the reprint order form by fax or by e-mail with the corrected proofs, to Wiley-VCH : [advenergymat@wiley.com](mailto:advenergymat@wiley.com)

**Corrections should be made directly in the PDF file using the PDF annotation tools. If you have questions about this, please contact the editorial office. The corrected PDF and any accompanying files should be uploaded to the journal's Editorial Manager site.**

To avoid commonly occurring errors, **please ensure that the following important items are correct** in your proofs (please note that once your article is published online, no further corrections can be made):

- **Names** of all authors present and spelled correctly
- **Titles** of authors correct (Prof. or Dr. only: please note, Prof. Dr. is not used in the journals)
- **Addresses** and **postcodes** correct
- **E-mail address** of corresponding author correct (current email address)
- **Funding bodies** included and grant numbers accurate
- **Title** of article OK
- All **figures** included
- **Equations** correct (symbols and sub/superscripts)

## Author Query Form

# WILEY

Journal            AENM  
 Article            aenm201901938

Dear Author,

During the copyediting of your manuscript the following queries arose.

Please refer to the query reference callout numbers in the page proofs and respond to each by marking the necessary comments using the PDF annotation tools.

Please remember illegible or unclear comments and corrections may delay publication.

Many thanks for your assistance.

Query No.	Description	Remarks
Q1	Please confirm that forenames/given names (blue) and surnames/family names (vermilion) have been identified correctly.	
Q2	Please provide the highest academic title (either Dr. or Prof.) for all authors, where applicable.	
Q3	Open access publication of this work is possible via Wiley OnlineOpen. Information about OnlineOpen, the article publication charges (APCs), and Wiley's agreements with various institutions to cover the APCs for their affiliated authors can be found at: <a href="https://authorservices.wiley.com/author-resources/Journal-Authors/licensing-open-access/open-access/onlineopen.html">https://authorservices.wiley.com/author-resources/Journal-Authors/licensing-open-access/open-access/onlineopen.html</a> .  The cost of publishing your manuscript OnlineOpen may be covered by one of Wiley's national agreements. To find out more, log in to your Wiley Author Services account or check the website: <a href="https://authorservices.wiley.com/author-resources/Journal-Authors/open-access/affiliation-policies-payments/index.html">https://authorservices.wiley.com/author-resources/Journal-Authors/open-access/affiliation-policies-payments/index.html</a> . Eligibility for these funds is based on the affiliation of the primary corresponding author.	
Q4	Please shorten Table of Contents text to a maximum of 60 words. All abbreviations should be defined.	
Q5	A footnote has been added in Table 1. Please verify.	
Q6	Please check all equations have been correctly typeset.	
Q7	Please confirm if the inserted page no. is correct in ref. [12].	
Q8	Please confirm if the inserted page no. is correct in ref. [13].	
Q9	Please update ref. [29] if already published.	
Q10	Please confirm if the inserted publisher name and publisher location is correct in ref. [32].	
Q11	Please confirm if the inserted page no. is correct in ref. [33].	
Q12	Please confirm if the inserted page no. is correct in ref. [35].	
Q13	Please confirm if the inserted page no. is correct in ref. [36].	
Q14	Please confirm if the inserted page no. is correct in ref. [42].	
Q15	Please confirm if the inserted page no. is correct in ref. [43].	
Q16	Please confirm if the updated bibliographic details are correct in ref. [44].	
Q17	Please confirm if the inserted page no. is correct in ref. [52].	
Q18	Please provide the publisher name and publisher location in ref. [53].	
Q19	Please provide the page no. in ref. [55].	
Q20	Please provide the complete bibliographic details in ref. [71].	

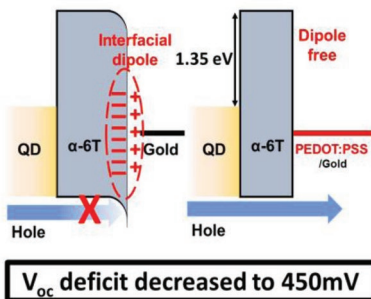
**Author: Please confirm that Funding Information has been identified correctly.**

Please confirm that the funding sponsor list below was correctly extracted from your article: that it includes all funders and that the text has been matched to the correct FundRef Registry organization names. If a name was not found in the FundRef registry, it may not be the canonical name form, it may be a program name rather than an organization name, or it may be an organization not yet included in FundRef Registry. If you know of another name form or a parent organization name for a "not found" item on this list below, please share that information.

FundRef Name	FundRef Organization Name
KIST	Korea Institute of Science and Technology
National Research Foundation of Korea	National Research Foundation of Korea
National Research Foundation of Korea (NRF)	National Research Foundation of Korea
Ministry of Science and ICT	

H. Lim, D. Kim, M.-J. Choi, E. H. Sargent,  
Y. S. Jung,\* J. Y. Kim\* ..... 1901938

**Suppressing Interfacial Dipoles  
to Minimize Open-Circuit Voltage Loss  
in Quantum Dot Photovoltaics**



Today, the open-circuit voltage ( $V_{OC}$ ) of state-of-the-art quantum dot photovoltaics (QD-PVs) remains low relative to its bandgap. In the present work, a bilayer hole-transport layer (HTL) with various band structures is developed and adapted to suppress undesired interfacial dipoles and electron leakage. The results reveal the relationship between electron blocking barrier at HTL and open-circuit voltage, which in turn enables a QD-PV cell with a  $V_{OC}$  deficit of 450 mV, one of the highest reported in literature to date.

Q4

UNCORRECTED PROOF

1  
2  
3  
4  
5  
6  
7  
8  
9  
10  
11  
12  
13  
14  
15  
16  
17  
18  
19  
20  
21  
22  
23  
24  
25  
26  
27  
28  
29  
30  
31  
32  
33  
34  
35  
36  
37  
38  
39  
40  
41  
42  
43  
44  
45  
46  
47  
48  
49  
50  
51  
52  
53  
54  
55  
56  
57  
58  
59

1  
2  
3  
4  
5  
6  
7  
8  
9  
10  
11  
12  
13  
14  
15  
16  
17  
18  
19  
20  
21  
22  
23  
24  
25  
26  
27  
28  
29  
30  
31  
32  
33  
34  
35  
36  
37  
38  
39  
40  
41  
42  
43  
44  
45  
46  
47  
48  
49  
50  
51  
52  
53  
54  
55  
56  
57  
58  
59

# Suppressing Interfacial Dipoles to Minimize Open-Circuit Voltage Loss in Quantum Dot Photovoltaics

Hunhee Lim, Donghun Kim, Min-Jae Choi, Edward H. Sargent, Yeon Sik Jung,\*  
and Jin Young Kim\*

Quantum-dot (QD) photovoltaics (PVs) offer promise as energy-conversion devices; however, their open-circuit-voltage ( $V_{OC}$ ) deficit is excessively large. Previous works have identified factors related to the QD active layer that contribute to  $V_{OC}$  loss, including sub-bandgap trap states and polydispersity in QD films. This work focuses instead on layer interfaces, and reveals a critical source of  $V_{OC}$  loss: electron leakage at the QD/hole-transport layer (HTL) interface. Although large-bandgap organic materials in HTL are potentially suited to minimizing leakage current, dipoles that form at an organic/metal interface impede control over optimal band alignments. To overcome the challenge, a bilayer HTL configuration, which consists of semiconducting alpha-sexithiophene ( $\alpha$ -6T) and metallic poly(3,4-ethylenedioxythiophene) polystyrene sulfonate (PEDOT:PSS), is introduced. The introduction of the PEDOT:PSS layer between  $\alpha$ -6T and Au electrode suppresses the formation of undesired interfacial dipoles and a Schottky barrier for holes, and the bilayer HTL provides a high electron barrier of 1.35 eV. Using bilayer HTLs enhances the  $V_{OC}$  by 74 mV without compromising the  $J_{SC}$  compared to conventional  $MoO_3$  control devices, leading to a best power conversion efficiency of 9.2% (>40% improvement relative to relevant controls). Wider applicability of the bilayer strategy is demonstrated by a similar structure based on shallow lowest-unoccupied-molecular-orbital (LUMO) levels.

Photovoltaic (PV) cells containing colloidal quantum dots (QDs) have recently garnered considerable attention owing to their potential as low-cost, large-scale, and air-stable

H. Lim, Prof. Y. S. Jung  
Department of Materials Science and Engineering  
Korea Advanced Institute of Science and Technology (KAIST)  
291 Daehak-ro, Yuseong-gu, Daejeon 305-701, Republic of Korea  
E-mail: ysjung@kaist.ac.kr

Dr. D. Kim  
Computational Science Research Center  
Korea Institute of Science and Technology (KIST)  
Seoul 02792, Republic of Korea

Dr. M.-J. Choi, Prof. E. H. Sargent  
Department of Electrical and Computer Engineering  
University of Toronto  
10 King's College Road, Toronto, Ontario M5S 3G4, Canada

Dr. J. Y. Kim  
Center for Hydrogen and Fuel Cell Research  
Korea Institute of Science and Technology (KIST)  
Seoul 02792, Republic of Korea  
E-mail: jinykim@kist.re.kr

The ORCID identification number(s) for the author(s) of this article can be found under <https://doi.org/10.1002/aenm.201901938>.

DOI: 10.1002/aenm.201901938

solar-energy-harvesting devices.<sup>[1–6]</sup> The power conversion efficiencies of QD-PV devices have been dramatically enhanced during the last decade, to the present-day record of over 12%, based on favorable optical properties including facile bandgap ( $E_g$ ) tunability and wide spectral responses.<sup>[7–9]</sup> Despite rapid improvements, the performance of QD-PVs is still below the expected level for an active material with this bandgap energy: a large open circuit voltage ( $V_{OC}$ ) deficit (defined as  $V_{SQ} - V_{OC}$ , where  $V_{SQ}$  is the Shockley–Queisser limit of  $V_{OC}$  for a given bandgap) remains a key bottleneck.<sup>[5,10]</sup> Even state-of-art PbS QD-PVs have  $V_{OC}$  deficits in the range of 400–550 mV, which is much larger than that (100–200 mV) of high-efficiency PV cells based on *c*-Si, GaAs, and hybrid perovskites.<sup>[11,12]</sup>

Previous works identified two QD-related factors responsible for the excessive  $V_{OC}$  loss: sub-bandgap trap states and polydispersity in QD films.<sup>[5,11–19]</sup> A high density of trap states can form in QD materials due to the large surface area and metal-to-chalcogen off-stoichiometry,<sup>[10,13,15]</sup> and recent works demonstrated that the reduction of the trap states via application of new surface passivation layers can increase the  $V_{OC}$  by  $\approx 100$  mV.<sup>[10,12]</sup> Another important factor underlying  $V_{OC}$  loss is energy disorder (i.e., bandtail states) within polydisperse QD films.<sup>[17]</sup> Synthetic modifications in the ligand exchange have recently enabled the realization of increased-monodispersity PbS QD films, and as a result  $V_{OC}$  enhancements of up to 90 mV were demonstrated in QD-PVs.<sup>[5,16]</sup>

Despite recent efforts to tune QD properties,  $V_{OC}$  loss is still too large, and there remains therefore a need to develop additional routes to further reduce the loss. Attempts thus far have concentrated mainly on tuning the QD layer only. Comparatively less attention has been paid to the interfaces between constituent layers in the device, although interface optimization is critical to controlling the device leakage current or interfacial recombination, and consequently the  $V_{OC}$ . In particular, there have been limited studies on the effect of band engineering at interfaces formed with the hole-transport layer (HTL) on PV performance. At present,  $MoO_3$ <sup>[20–22]</sup> and ethanedithiol (EDT)-passivated QDs (EDT-QDs)<sup>[5,6]</sup> are the most widely used HTL materials in the QD-PV field. However, these materials provide an insufficiently large energy barrier for electron of 0.2–0.4 eV

(both in our measurements and literature<sup>[6,23]</sup>), inadequate to block electron leakage.

Large-bandgap organic or conjugated polymer materials are typically characterized by shallow lowest-occupied-molecular-orbital (LUMO) levels, and thus are potentially ideal for HTLs to block electron leakage. These materials, however, often form strong dipole moments at interfaces with metal electrodes in devices,<sup>[23–25]</sup> which impedes control toward optimal band alignments. In this work, to overcome this challenge, we develop a novel bilayer HTL that consists of semiconducting alpha-sexithiophene ( $\alpha$ -6T) and metallic poly(3,4-ethylenedioxythiophene) polystyrene sulfonate (PEDOT:PSS). The introduction of the buffer PEDOT:PSS between  $\alpha$ -6T and the Au electrode suppresses the formation of undesired interfacial dipoles and a Schottky barrier for holes, and the bilayer HTL provides a large electron barrier of 1.35 eV. The bilayer HTL enhances the  $V_{OC}$  by 74 mV with no  $J_{SC}$  sacrifice, compared to control devices, owing to a reduction of the dark leakage current. Moreover, PV devices based on the new HTL are highly stable in air for more than 400 h. We demonstrate that the bilayer HTL strategy is applicable to other small molecules or conjugated polymers that are also characterized by a shallow LUMO. This work reveals that the  $V_{OC}$  deficit in QD-PVs is increased by electron leakage at the QD/HTL interface, and suggests a practical solution to minimize the loss.

Today, most advanced QD-PV devices utilize either  $MoO_3$  or EDT-passivated QDs (EDT-QDs) materials as the HTL (Figure 1a). For selective and efficient hole extraction, the HTL should satisfy the following three requirements: 1) no barrier for holes, 2) large enough barrier for electrons (desirably  $>1.0$  eV), and 3) high hole mobility ( $\mu_h > 10^{-3}$  cm<sup>2</sup> V<sup>-1</sup> s<sup>-1</sup>). Although both  $MoO_3$  and EDT-QD satisfy the requirement of the absence of an energy barrier for hole conduction, the other important requirements are not met. For the case of EDT-QD in the HTL, the energy barrier for electrons was measured to be only 0.17 eV, which is not large enough to effectively suppress electron leakage (Figure S1, Supporting Information). Furthermore, the hole mobility of  $MoO_3$  and EDT-QD was estimated to be extremely low, only  $7 \times 10^{-5}$  and  $1 \times 10^{-4}$  cm<sup>2</sup> V<sup>-1</sup> s<sup>-1</sup>, respectively.<sup>[26,27]</sup> These properties raise substantive concerns that conventional HTLs may not function properly, likely leading to considerable loss in  $V_{OC}$  and  $J_{SC}$ .

It is therefore imperative to identify HTL materials that fulfill the aforementioned three requirements. We focused on small organic molecules and conjugated polymers that are typically characterized by shallow LUMO levels. We built a library of 36 materials, where the energy levels [highest-occupied-molecular-orbital (HOMO) and LUMO levels] and hole mobilities are collected from the literature (Figure 1b,c).<sup>[20,21,27–64]</sup> To perform sequential screening, we defined quantitative criteria as follows: 1)  $-5.6$  eV  $<$  HOMO  $<$   $-5.1$  eV (no barrier for holes), 2)  $-3.6$  eV  $<$  LUMO (barrier for electrons  $>0.75$  eV), and 3)  $\mu_h > 1.0 \times 10^{-3}$  cm<sup>2</sup> V<sup>-1</sup> s<sup>-1</sup>. Materials having a HOMO level shallower than  $-5.1$  eV should also be screened in order to avoid a barrier with an adjacent electrode material (work function of Au =  $-5.1$  eV). Based on the screening criteria, we considered the following eight materials as promising HTL materials, in order from shallow to deep LUMO: 5,10,15-tribenzyl-5H-diindolo[3,2- $\alpha$ :3',2'-c] carbazole (TBDI), 5,10,15-triphenyl-5H-diindolo[3,2- $\alpha$ :3',2'-c]

carbazole (TPDI),  $\alpha$ -6T, poly(3-hexylthiophene) (P3HT), poly[[4,8-bis[(2-ethylhexyl)oxy]benzo[1,2- $b$ :4,5- $b'$ ]dithiophene-2,6-diyl][3-fluoro-2-[(2-ethylhexyl)carbonyl]thieno[3,4- $b$ ]thiophenediyl]] (PTB7), poly(2,6-bis(thiophen-2-yl)-3,5-didecanyldithieno[3,2- $b$ :20,30- $d$ ]thiophene)-3,6-bis(5-bromo-2-thienyl)-2,5-dihydro-2,5-diethylhexylpyrrolo[3,4- $c$ ]pyrrole-1,4-dione (PTDTTDDPP), poly[N-9'-hepta-decanyl-2,7-carbazole-alt-5,5-(4',7'-di-2-thienyl-2',1',3'-benzothiadiazole)] (PCDTBT), and poly[2,6-(4,4-bis-(2-ethylhexyl)-4H-cyclopenta[2,1- $b$ :3,4- $b'$ ]dithiophene)-alt-4,7(2,1,3-benzothiadiazole)] (PCPDTBT). We mainly focused on using  $\alpha$ -6T to demonstrate enhanced PV performance, although we also tested other materials to verify wide applicability of this strategy.

When an organic or conjugated polymer material ( $\alpha$ -6T in this case) forms a junction with a metal (Au electrode, in this case) in PV devices, the energy levels at the interface may be substantially shifted due to dipole formation at the organic/metal interface.<sup>[23–25]</sup> This property could severely limit the potential of these organic/polymer materials in the HTL of QD-PV devices. In our ultraviolet photoelectron spectroscopy (UPS) measurements (Figure S2, Supporting Information), a substantial downward shift ( $\approx 0.65$  eV) of the vacuum energy level compared to that of noninteractive state (Figure 2a) was indeed observed for  $\alpha$ -6T when in a direct contact with Au. This results in the formation of Schottky barriers (0.65 eV) for holes at the interface between the Au electrode and  $\alpha$ -6T, and thus the hole extraction from  $\alpha$ -6T to the Au electrode is undesirably blocked (Figure 2b). The PV devices fail to perform when an Au electrode and  $\alpha$ -6T forms a direct junction (Figure S3, Supporting Information).

In order to overcome this critical issue, we investigated the insertion of the metallic polymer PEDOT:PSS between  $\alpha$ -6T and Au. We hypothesized that PEDOT:PSS, as a polymer material, would form a much weaker interfacial dipole with  $\alpha$ -6T, and at the same time, it is compatible with Au due to its metallic band structure. UPS measurements revealed a negligible shift of energy levels of  $\alpha$ -6T after the insertion of the PEDOT:PSS layer (Figure S4, Supporting Information) due to the reduction of the interfacial dipole (Figure 2c). The combined use of PEDOT:PSS (i.e., bilayer HTL) therefore suppresses the formation of the dipole-induced Schottky barrier for holes, and consequently allows facile hole transport from  $\alpha$ -6T HTL to the Au electrode.

To clarify the role of the PEDOT:PSS insertion in reducing interfacial dipoles, we performed density-functional-theory (DFT) calculations for several interfacial material systems. It is necessary to compare the energy level shifts at Au/ $\alpha$ -6T versus Au/PEDOT:PSS/ $\alpha$ -6T system. For the latter case, two interfaces, i.e., PEDOT:PSS/ $\alpha$ -6T and Au/PEDOT:PSS, should separately be investigated.

First of all, the interfacial dipoles occurring at each Au/ $\alpha$ -6T and PEDOT:PSS/ $\alpha$ -6T interface are compared. Since PEDOT:PSS is composed of PEDOT and PSS in different ratios,<sup>[65,66]</sup> we built separate organic/polymer interfaces with each of PEDOT/ $\alpha$ -6T and PSS/ $\alpha$ -6T,<sup>[67]</sup> and also with Au(111)/ $\alpha$ -6T for comparison (Figure 2d). Figure 2e shows the interface-induced change of the electrostatic potentials of  $\alpha$ -6T for these three interfaces.<sup>[22]</sup> The vacuum energy levels (flat potential lines in vacuum region) highlight the different

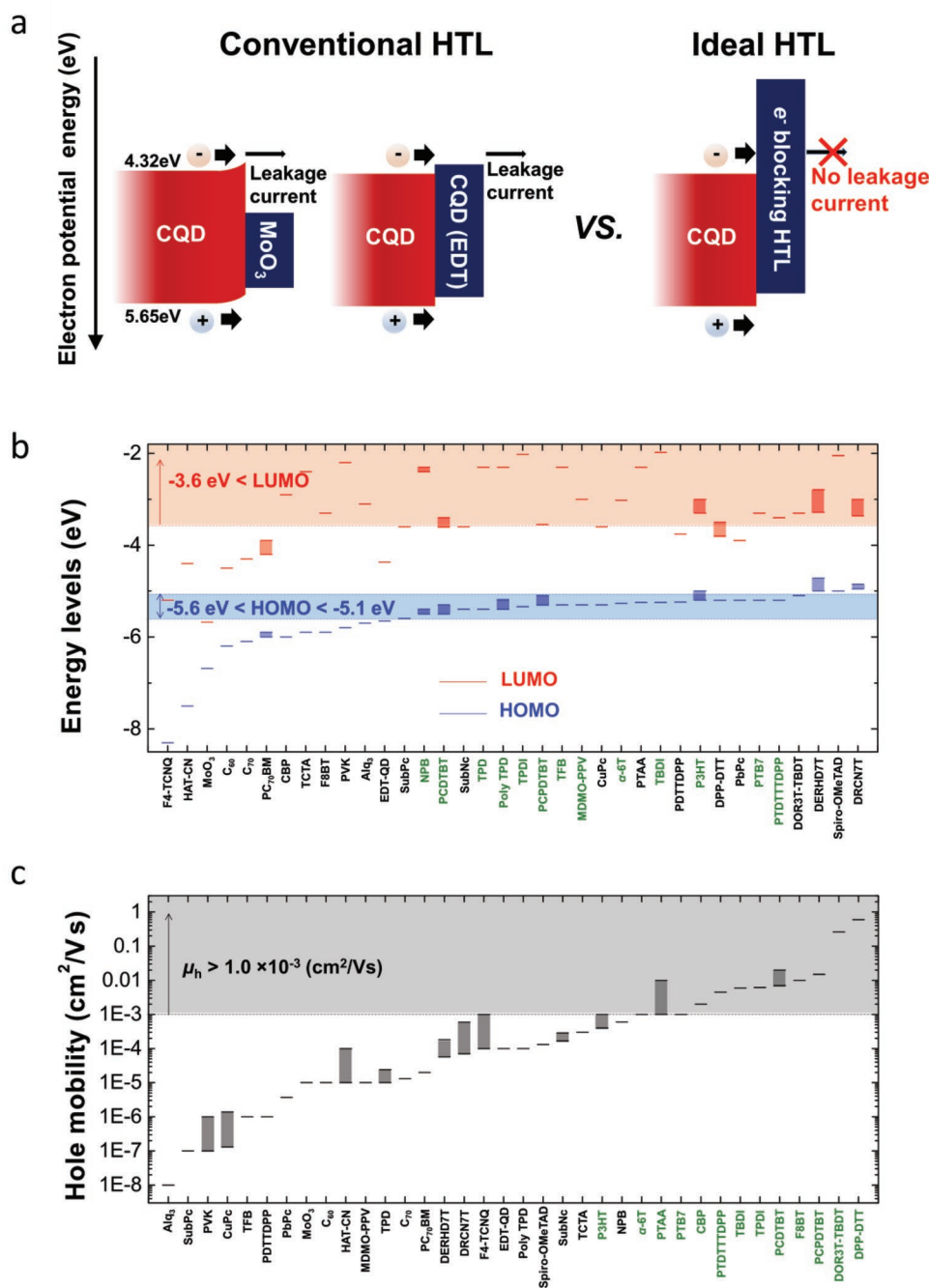


**Figure 1.** In search of HTL materials toward high-performance QD-PVs. a) Band alignments of conventional versus ideal hole-transport materials for effective charge-carrier collection in QD-PVs, with a particular focus on the barrier formed at the QD/HTL interface. b) LUMO and HOMO levels of candidate HTL materials, collected from the literature.<sup>[21,22,25–62]</sup> The materials are listed in the order of deep to shallow HOMO levels. The blue and red blocks shaded over the entire materials denote the ideal range for HOMO and LUMO levels, respectively. c) Hole mobility of candidate HTL materials, collected from the literature. The materials are listed in the order of low to high mobility. The gray block shaded over the entire materials denotes the ideal range for hole mobility.

vacuum energy shifts ( $\Delta E_{vac}$ ). A large  $\Delta E_{vac}$  of around  $-0.74$  eV is observed for Au/ $\alpha$ -6T, whereas it is much smaller in magnitude ( $+0.15$  and  $+0.06$  eV) for other PEDOT/ $\alpha$ -6T and PSS/ $\alpha$ -6T interfaces, respectively. The DFT results of  $\Delta E_{vac}$  agree well with the UPS measurement results qualitatively. The difference in  $\Delta E_{vac}$  between Au and PEDOT:PSS originates from the different

degree of electron transfer (Figure 2f,i). For Au(111)/ $\alpha$ -6T, particularly strong Au-S chemical bonds form, which is favorable to facilitate electron transfer. For the other two interfaces (PEDOT/ $\alpha$ -6T and PSS/ $\alpha$ -6T), much weaker van der Waals forces are the primary interactions, which restrict the interfacial charge transfer.

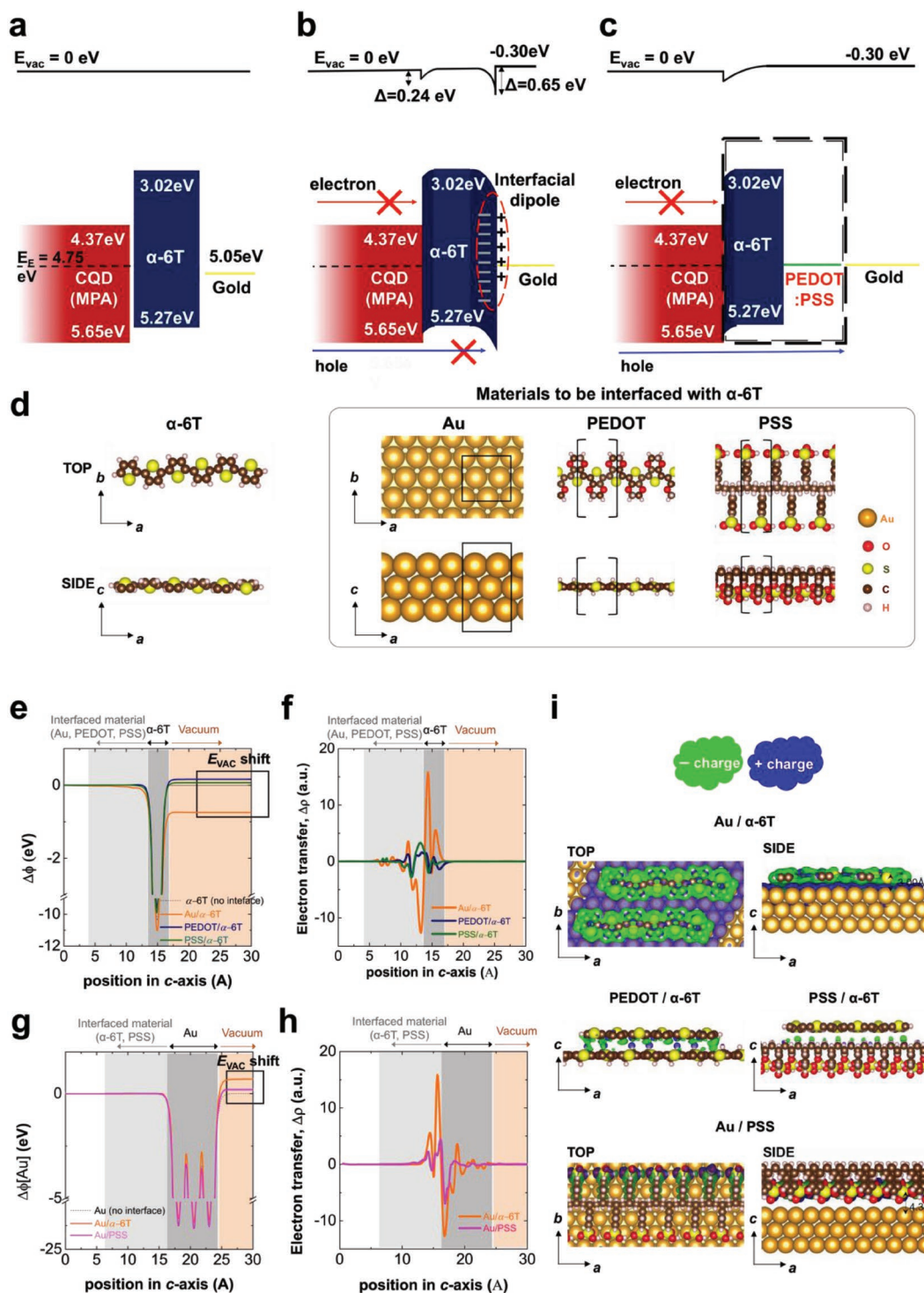


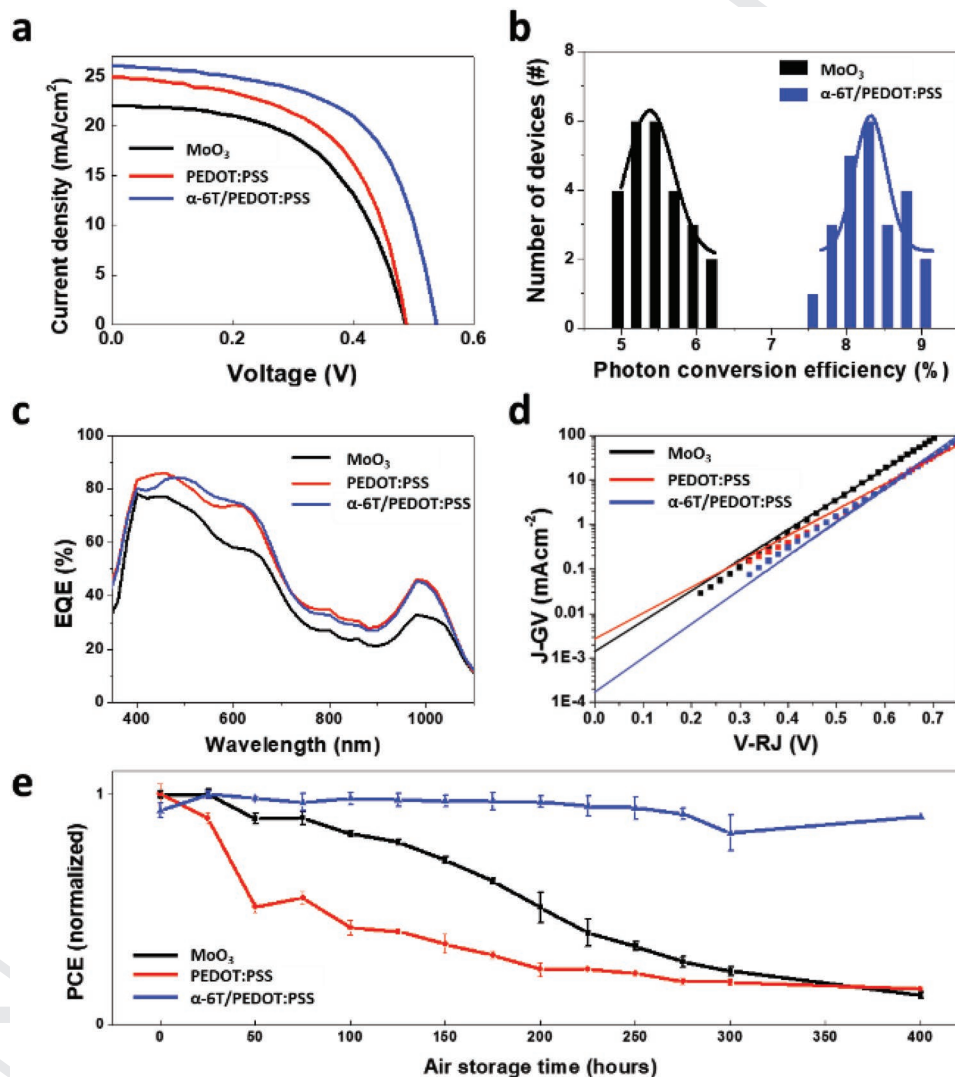
**Figure 2.** A combined UPS and DFT study to calculate the band structures of QDs, HTL, and electrode in QD-PVs. a–c) Schematics of band diagrams obtained by UPS measurement when each layer is separate a), in contact, when only  $\alpha$ -6T is used for the HTL b), in contact, when bilayer materials ( $\alpha$ -6T/PEDOT:PSS) are used for the HTL (c), respectively, with a particular focus on interfacial dipoles and related energy-level shift. All numbers in the energy diagrams are calculated with respect to the vacuum energy level of the CQD layer. Note that the dipoles only affect the energy level shifts in the corresponding interfacial regions. d–i) DFT simulation results. d) Each molecular or crystal structure used in DFT simulations of  $\alpha$ -6T, Au(111), PEDOT, PSS, e) Interface-induced change in the electrostatic potential of the  $\alpha$ -6T system plotted along the  $c$ -axis (i.e.,  $ab$ -plane averaged), or  $\Delta\phi[\alpha\text{-6T}] = \phi_{\text{total}} - \phi_{\text{interfacial-material}}$ . f) Interface-induced electron transfer plotted along the  $c$ -axis, or  $\Delta\rho = \rho_{\text{total}} - [\rho_{\text{interfacial-material}} + \rho_{\alpha\text{-6T}}]$ . g) Interface-induced change in the electrostatic potential of the Au(111) system plotted along the  $c$ -axis, or  $\Delta\phi[\text{Au}] = \phi_{\text{total}} - \phi_{\text{interfacial-material}}$ . h) Interface-induced electron transfer plotted along the  $c$ -axis, or  $\Delta\rho = \rho_{\text{total}} - [\rho_{\text{interfacial-material}} + \rho_{\text{Au}}]$ . i) 3D visualizations of the charge transfer for four modeled interfaces.

1 Second, the interfacial dipoles occurring at each Au/ $\alpha$ -6T  
2 and Au/PEDOT:PSS interface are compared. It is well known  
3 that due to vertically phase-segregated PEDOT:PSS, a highly  
4 PSS-rich layer forms an interface with the metal electrode (in  
5 this case, Au electrode).<sup>[65,68]</sup>

6 We thus performed the simulation for the Au/PSS interface  
7 with Au/ $\alpha$ -6T as a comparison. Figure 2g shows the interface-  
8 induced change of the electrostatic potentials of Au for these  
9 two interfaces. The results reveal that a much weaker dipole  
10 forms at the Au/PSS interface ( $\Delta E_{\text{vac}}$  of 0.19 eV in the high-  
11 lighted box in Figure 2g) than the Au/ $\alpha$ -6T case (0.74 eV),  
12 which qualitatively agrees with UPS measurements (Figure S2,  
13 Supporting Information). This is because the sulfonate ( $\text{SO}_3^-$ )  
14 geometry in PSS and gold bonds is much weaker bonding than  
15 direct Au-S bonds. The calculated Au-S distance is 4.34 Å at  
16 the Au/PSS interface, which is much larger than 3.00 Å in the  
17 Au/ $\alpha$ -6T case (Figure 2h,i). Overall, our simulations support  
18

19 the experimental results that the insertion of PEDOT:PSS  
20 weakens the dipoles on both sides with Au and  $\alpha$ -6T, and dem-  
21 onstrate how PEDOT:PSS can suppress the formation of the  
22 undesired Schottky barrier for holes.

23 The incorporation of the new bilayer HTL ( $\alpha$ -6T/  
24 PEDOT:PSS) substantially improved the performance of  
25 QD-PVs, compared to the control devices based on  $\text{MoO}_3$ ,  
26 HTL (Figure 3a and Table 1). The  $J$ - $V$  curves in Figure 3a  
27 reveal that the use of the bilayer HTL improved the  $V_{\text{OC}}$  by  
28 74 mV and  $J_{\text{SC}}$  by 3.5  $\text{mA cm}^{-2}$ , leading to a best power con-  
29 version efficiency (PCE) of 9.2%. The PCE enhancement is  
30 a general observation, confirmed from more than 30 device  
31 samples (Figure 3b). Importantly, it should be noted that  
32 enhancements of the performance factors ( $V_{\text{OC}}$ ,  $J_{\text{SC}}$ , fill  
33 factor) are also observed when EDT-QDs are used as the control  
34 HTL material, instead of  $\text{MoO}_3$  (Figure S5, Supporting  
35 Information).  
36  
37  
38  
39  
40  
41  
42  
43  
44  
45  
46  
47  
48  
49  
50  
51  
52  
53  
54  
55  
56



56 **Figure 3.** QD-PV performance, characterizations, and air stability. a)  $J$ - $V$  curves of the devices with different HTL materials ( $\text{MoO}_3$ , PEDOT:PSS alone,  
57 and  $\alpha$ -6T/PEDOT:PSS). b) A histogram highlighting the PCE distributions of PV devices obtained from numerous experimental tests. c) External  
58 quantum efficiency (EQE) of the PV devices. d)  $J$ -GV versus  $V$ -RJ graphs of the PV devices to obtain dark leakage current ( $J_0$ , the intercept at  $y$ -axis),  
59 where  $G$  and  $R$  refer to conductance and resistance, respectively. e) Stability tests of the PV devices stored in air for 400 h.



**Table 1.** Statistical performance data of QD-PV devices with different HTL materials.

	<sup>a)</sup> $V_{OC}$ [V]	$J_{SC}$ [mA cm <sup>-2</sup> ]	Fill factor [%]	PCE (%)	$J_0$ (mA cm <sup>-2</sup> )
MoO <sub>3</sub>	0.50 ± 0.02 (0.52)	20.7 ± 1.2 (21.3)	55.9 ± 4.5 (58.6)	5.8 ± 0.4 (6.4)	1.5 ± 0.3 × 10 <sup>-3</sup>
PEDOT:PSS	0.52 ± 0.02 (0.53)	24.2 ± 1.3 (23.6)	56.3 ± 2.8 (60.5)	7.0 ± 0.3 (7.6)	1.3 ± 0.2 × 10 <sup>-3</sup>
α-6T/PEDOT:PSS	0.57 ± 0.02 (0.57)	24.2 ± 1.5 (25.6)	60.0 ± 2.4 (62.7)	8.3 ± 0.5 (9.2)	2.7 ± 0.2 × 10 <sup>-4</sup>

<sup>a)</sup>Each PV performance parameter is averaged over 30 samples.  $J_0$  is averaged from 5 samples. The numbers in the parentheses are the values of the best performing device.

We also compare the performance of the bilayer HTL structure with that of single-layered HTLs, i.e., PEDOT:PSS or α-6T layer alone. Using single-layer PEDOT:PSS with a higher hole mobility improved only the  $J_{SC}$  (no  $V_{OC}$  enhancement). This indicates that the observed  $J_{SC}$  enhancement for the bilayer HTLs case is mainly due to the increased hole mobility of the PEDOT:PSS layer. The external quantum efficiency (EQE) results presented in Figure 3c also clarify the origins of the  $J_{SC}$  enhancements. The PEDOT:PSS and α-6T/PEDOT:PSS exhibit larger EQE values than the MoO<sub>3</sub> case over the entire wavelength range. Second, simply replacing MoO<sub>3</sub> with α-6T results in unacceptably inefficient device performance (PCE ≈ 0.24%, Figure S3, Supporting Information). This result can be explained by the energy band diagram (Figure 2b) determined from the UPS measurement data. The diagram shows that hole extraction from QDs is undesirably blocked due to the substantial downward shift of the vacuum energy level of α-6T. These comparisons of device performance confirm that the combined use of α-6T and PEDOT:PSS in HTL is indeed beneficial.

To investigate any connection between the  $V_{OC}$  improvement in the bilayer HTL and the existence of electron leakage, we acquired dark  $J$ - $V$  characteristics.  $V_{OC}$  is inversely related to the dark current density ( $J_0$ ) as follows

$$V_{OC} = \frac{nkT}{q} \ln \left( \frac{J_{SC}}{J_0} \right) \quad (1)$$

where  $n$  is the diode ideality factor,  $k$  is the Boltzmann constant,  $T$  is the temperature,  $q$  is the electric charge constant. The total dark diode current can be expressed

$$J = J_0 \exp \left[ \frac{q}{nkT} (V - RJ) \right] + GV \quad (2)$$

where  $R$  is the series resistance and  $G$  is the shunt conductance. In the graph of  $J$ - $GV$  versus  $V$ - $RJ$  in Figure 3d,  $J_0$  was determined as the value of the  $y$ -intercept (at  $V$ - $RJ = 0$ ). Devices using MoO<sub>3</sub> or PEDOT:PSS alone for HTL produced a dark current density ( $J_0$ ) of around  $1.2 \times 10^{-3}$ – $1.5 \times 10^{-3}$  mA cm<sup>-2</sup>. On the other hand, the device using the bilayer HTL of α-6T/PEDOT:PSS exhibited notably reduced (about 1/5) leakage current density ( $2.7 \times 10^{-4}$  mA cm<sup>-2</sup>).

The quantitative impact of  $J_0$  reduction on  $V_{OC}$  enhancement is assessed using Equation (1). Based on the measured  $J_0$  and  $J_{SC}$  values (Table 1), the term  $n \ln(J_{SC}/J_0)$  for the bilayer HTL device was estimated to be 8.1% and 16.1% larger than those of the cases of PEDOT:PSS and MoO<sub>3</sub> alone, respectively. These values agree well with the  $V_{OC}$  enhancements in the device characterization results, improvements of 10.9% (compared

to PEDOT:PSS alone) and 14.9% (compared to MoO<sub>3</sub> alone). These quantitative comparisons indicate that the observed  $V_{OC}$  improvements can be ascribed to the reduced leakage current in dark, enabled by the introduction of the substantial electron blocking barrier of 1.5 eV by the new bilayer HTL. These results support that electron leakage in the dark at the QD/HTL interface is an important  $V_{OC}$  loss mechanism.

Another beneficial result of the bilayer HTL is long-term air stability of PV devices. The devices with three different HTLs (i.e., MoO<sub>3</sub>, PEDOT:PSS, and α-6T/PEDOT:PSS) were stored in air for 400 h, and the PV device performance was measured on a daily basis. Figure 3e shows the history of PV performance over time. The new bilayer HTL of α-6T/PEDOT:PSS substantially improved the PV device stability in air, compared to the case of MoO<sub>3</sub> or PEDOT:PSS alone. For the new bilayer HTL, the average PCE remained constant even following 400 h air storage, while a substantial drop in the PCE was observed for the other cases (both PCEs dropped to below 15% of initial performance after 400 h). The poor air stability of the MoO<sub>3</sub> device is consistent with previous studies, and the degradation can be attributed to the MoO<sub>3</sub> being highly vulnerable to oxidation.<sup>[69]</sup> The use of PEDOT:PSS is also known to degrade the devices due to its acidic and hygroscopic nature.<sup>[70,71]</sup> In other words, the PbS QDs in contact with PEDOT:PSS will likely be susceptible to oxidation. For the α-6T/PEDOT:PSS case, however, the insertion of α-6T layer blocks the direct contact between the QDs and PEDOT:PSS layer, markedly improving air stability.

To demonstrate the wide applicability of the bilayer HTL strategy, we also considered other materials (TBDI, TPD1, P3HT, PTB7, PTDTTDDPP, PCDTBT, and PCPDTBT) chosen via the aforementioned screening process (Figure 1b,c). We tested QD-PV devices with two polymer HTL materials, i.e., P3HT and PCPDTBT, both of which satisfy the requirements of HOMO/LUMO levels and hole mobility. Similar to the α-6T case, the PV devices with P3HT or PCPDTBT alone in HTL do not function properly, likely due to the dipole-induced Schottky barrier for holes (Figure 4a). To prevent the substantial interfacial dipole between these polymers and Au electrode, PEDOT:PSS is also inserted in each case. Therefore, additional bilayer HTL structures, P3HT/PEDOT:PSS and PCPDTBT/PEDOT:PSS, are tested. Using bilayer HTL leads to the efficient PV functioning for all cases (Figure 4a). It is important to note that  $V_{OC}$  enhancements are observed for these two HTLs (by 66 mV for the former and by 33 mV for the latter), compared to the control device of PEDOT:PSS alone, with no compromise to  $J_{SC}$  for all.

In Figure 4b,  $V_{OC}$  enhancements are shown as a function of the electron blocking barrier at the QD/HTL junction for each small molecule or conjugated polymer case (α-6T, P3HT,

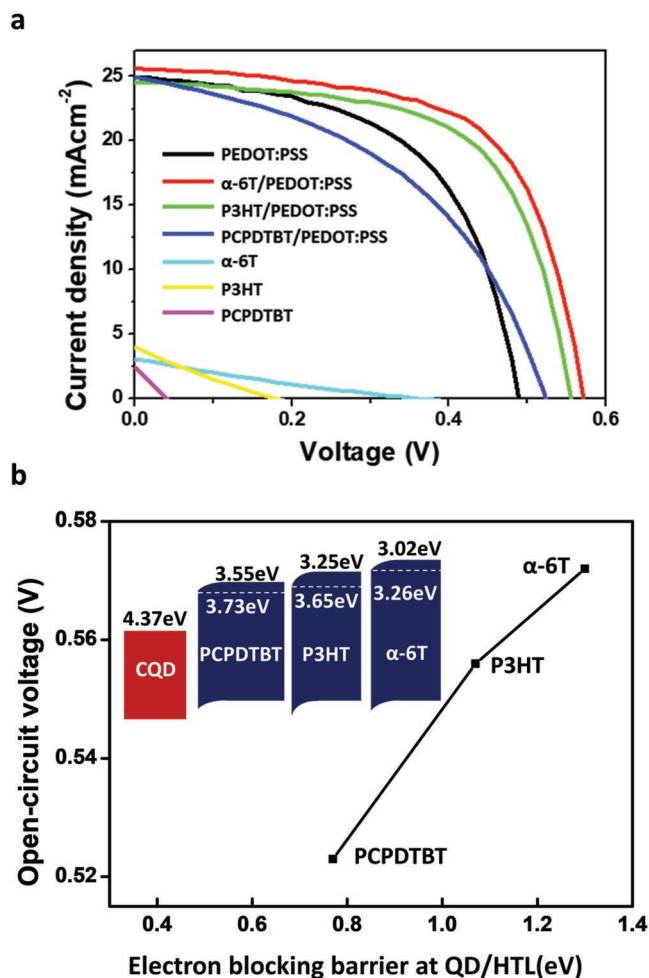


**Figure 4.** Extended applicability of the bilayer HTL strategy for  $V_{OC}$  enhancement. a) P3HT and PCPDTBT are further selected for these tests, as they satisfy the requirements of an ideal HTL (Figure 1).  $J$ - $V$  characteristics of each HTL material are shown and compared. b)  $V_{OC}$  enhancements are plotted as a function of the electron blocking barrier at each QD/HTL junction.

and PCPDTBT) in the bilayer HTL. The electron blocking barrier at the QD/HTL junction can be estimated by the difference between the LUMO level of the HTL material and the CBM level of the QD layer, i.e.,  $\Delta = \text{LUMO (HTL)} - \text{CBM (QD)}$ . A positive correlation between  $\Delta$  and  $V_{OC}$  enhancement is observed in Figure 4b, supporting that the  $V_{OC}$  deficit in QD-PV is quantitatively impacted by electron leakage at the QD/HTL interface. This result suggests that small molecules or conjugated polymers characterized by shallow LUMO levels are more effective in reducing the electron leakage, and thus should be prioritized in the design of the bilayer HTL. Overall, the improvements in  $V_{OC}$ ,  $J_{SC}$ , and air stability support that our work provides a properly designed HTL scheme to enhance the competitiveness of QD-PVs.

In summary, this study reveals that electron leakage at the interface between QDs and the HTL causes excessive  $V_{OC}$  loss in conventional QD-PVs. Owing to their shallow LUMO levels and high hole mobilities, some conjugated small molecules including  $\alpha$ -6T are potentially suited for minimizing

the leakage currents; however, interfacial dipoles formed at the metal-organic semiconductor junction produce a Schottky barriers for holes and hinder the PV functioning. In our case, the dipole formed at the interface between  $\alpha$ -6T and the Au electrode forms a Schottky barrier of 0.65 eV, which impedes efficient hole extraction. To overcome this issue, we developed bilayer HTLs wherein a conducting polymer (PEDOT:PSS) buffer layer was introduced between  $\alpha$ -6T and the Au electrode, which in turn substantially relieves the interfacial dipoles. We confirm that our bilayer HTL comprising sequential  $\alpha$ -6T and PEDOT:PSS layers effectively suppress the undesired Schottky barrier for holes while providing a high electron blocking barrier of 1.35 eV.

The bilayer HTL experimentally improved the  $V_{OC}$  by 74 mV in QD-PVs (without compromising  $J_{SC}$ ), compared to the reference MoO<sub>3</sub> HTL case. This strategy is compatible with other previous achievements based on QD ligand engineering (e.g., EDT-passivated QDs as the reference HTL). We confirm that the sufficiently large electron blocking barrier ( $\approx 1.5$  eV) of the bilayer HTL reduces the dark leakage current by a factor of 5, which is quantitatively well correlated with the  $V_{OC}$  enhancements observed in the device characterization. Additionally, the new HTL offers considerably improved PV device stability in air, reaching more than 400 h. Few studies have achieved simultaneous improvements in  $V_{OC}$ ,  $J_{SC}$ , and air stability without a trade-off, and this is a unique strength of the new HTL scheme. By confirming analogous effects in  $V_{OC}$  improvements, we further demonstrated that our bilayer HTL strategy is widely applicable to other conjugated polymers and small molecules characterized by shallow LUMO levels.

## Experimental Section

**Density-Functional-Theory Calculations:** All the calculations were performed using the Vienna Ab Initio Simulation Packages (VASP)<sup>[72]</sup> with an energy cutoff of 480 eV. The projector-augmented-wave (PAW) method was adopted to describe the potential of the ionic cores.<sup>[73]</sup> The generalized gradient approximation of revised Perdew–Burke–Ernzerhof (rPBE) was employed for the exchange and correlation functional.<sup>[74]</sup> van der Waals corrections were included. For Au slab system, (111) surface was chosen since it was known as the most stable low-index surface. For the Au/ $\alpha$ -6T system, a  $6 \times 1$  supercell of Au (111) unit (35.8 Å in  $a$ -axis) was built to make an interface with the  $\alpha$ -6T molecule (i.e., Au/ $\alpha$ -6T), as shown in Figure 2g. The Monkhorst–Pack  $k$ -point sampling of  $1 \times 3 \times 1$  was used. For the Au/PSS system, a  $5 \times 2$  supercell of Au (111) unit (29.8 Å in  $a$ -axis) was built to make an interface with the PSS polymer (i.e., Au/PSS). The Monkhorst–Pack  $k$ -point sampling of  $2 \times 2 \times 1$  was used. For both Au/ $\alpha$ -6T and Au/PSS systems, each Au (111) slab consisted of three single layers, where the bottom layer was not allowed to relax. That is,  $\alpha$ -6T, PSS, and the top two layers of the Au slab were fully relaxed. For the other two interfacial systems, or  $\alpha$ -6T/PEDOT and  $\alpha$ -6T/PSS interfaces were tested, and the geometry having minimum energy was selected and shown in Figure 2g. For these two systems, the Monkhorst–Pack  $k$ -point sampling of  $1 \times 1 \times 1$  was used. The geometry relaxation was accomplished using the conjugate gradient method until the maximum forces acting on each atom become less than 0.02 eV Å<sup>-1</sup>. Dipole corrections were included to remove the spurious electrostatic interactions between neighboring supercells.

**Materials:** Lead(II) oxide powder (PbO) (99%), 1-octadecene (ODE) (technical grade 90%), oleic acid (OA) (technical grade 90%), oleylamine (OLA) (technical grade 70%), hexamethyldisilathiane

1 ((TMS)<sub>2</sub>S) (synthesis grade), tetrabutylammonium iodide  
2 (TBAI) (99%), mercaptopropionic acid (MPA), and alpha-  
3 sexithiophene ( $\alpha$ -6T) were purchased from Sigma-Aldrich and poly  
4 (3,4-ethylenedioxythiophene)-poly(styrenesulfonate) (PEDOT:PSS) was  
5 purchased from Heraeus.

6 **Synthesis of PbS Quantum Dots:** The synthesis method was adapted  
7 from the literature.<sup>[75]</sup> Lead oxide (0.9 g) was dissolved in ODE (25 mL)  
8 with OA (2.7 mL). The solution was degassed and stirred overnight  
9 at 100 °C. Afterward, the lead precursor solution was degassed with  
10 nitrogen and the temperature was increased to 120 °C. The sulfur  
11 precursor was prepared by dissolving hexamethyldisilathiane (360  $\mu$ L)  
12 in ODE (10 mL). The lead precursor solution was vigorously stirred  
13 while the sulfur precursor solution was swiftly injected and cooled  
14 to 35 °C. The QDs were extracted and purified by acetone followed by  
15 centrifugation. The QDs were re-dissolved in toluene and washed three  
16 times by acetone and methanol followed by centrifugation. Finally, the  
17 QDs were dispersed in octane with concentration of 50 mg mL<sup>-1</sup> and  
18 stored in a glovebox.

19 **Synthesis of ZnO Nanoparticles:** The synthesis method was adapted  
20 from the literature.<sup>[6]</sup> Zinc acetate (2.95 g) was dissolved in methanol  
21 (125 mL) at 60 °C. Another solution of potassium hydroxide (1.48 g)  
22 was dissolved in methanol (65 mL). The solution with potassium  
23 hydroxide was slowly added to the zinc acetate solution and the injection  
24 was terminated after 10 min. The solution was continuously stirred at  
25 60 °C for 2.5 h. Afterward, the solution was extracted by centrifugation  
26 and the precipitants were washed twice by methanol followed by  
27 centrifugation. The precipitants were kept wet with methanol and  
28 dissolved in chloroform (10 mL). The final solution was filtered and kept  
29 in a refrigerator.

30 **Device Fabrication:** The ITO substrate was cleaned with solvents and  
31 treated with UV ozone. The ZnO solution was spin-coated to fabricate  
32 a 60 nm thick film. PbS QD films were deposited by layer-by-layer spin  
33 coating. 15  $\mu$ L of PbS QD solution was spin coated onto the substrate  
34 at 2500 rpm for 15 s. The PbS QD film was then soaked by TBAI  
35 solution (10 mg mL<sup>-1</sup> in methanol) for 30 s and washed with methanol  
36 three times. The TBAI-QD film fabrication process was repeated eight  
37 times (final thickness = 180 nm). For MPA-QD layers, a MPA solution  
38 (10 mg mL<sup>-1</sup> in methanol) was used and the process was repeated two  
39 times (final thickness = 40 nm). MoO<sub>3</sub> (20 nm),  $\alpha$ -6T (50 nm), and a  
40 gold/silver (40 nm/180 nm) electrode were deposited by a thermal  
41 evaporator at a pressure below  $1 \times 10^{-5}$  torr. The PEDOT:PSS solution  
42 (purchased solution was diluted by methanol by 33% in volume fraction)  
43 was spin coated at 5000 rpm for 60 s.

44 **Device Characterization:** A UV-vis spectrophotometer (Mecasys,  
45 Optizen POP, Korea) was used to obtain UV-vis absorption spectra of  
46 PbS QDs. A scanning electron microscope (FE-SEM, Hitachi, S-4800)  
47 was used to observe the cross-section of the QD film. A Keithley 2450  
48 source meter was used to obtain the current-voltage characteristics. J-V  
49 sweeps were performed in a N<sub>2</sub> filled glove box. A 150 W Xe lamp with  
50 an AM 1.5G filter (LS-150-Xe, Abet Technologies) was used to illuminate  
51 the device.

## Supporting Information

52 Supporting Information is available from the Wiley Online Library or  
53 from the author.

## Acknowledgements

54 H.L. and D.K. contributed equally to this work. This work was supported  
55 by KIST Institutional Program (2E28271) and Creative Materials  
56 Discovery Program through the National Research Foundation of Korea  
57 (NRF-2016M3D1A1021140), the Creative Material Discovery Program  
58 through the National Research Foundation of Korea (NRF) funded by  
59 Ministry of Science and ICT (NRF-2016M3D1A1900035).

## Conflict of Interest

The authors declare no conflict of interest.

## Keywords

band engineering, hole transport layer, interfacial dipole, quantum dot  
solar cell

Received: June 17, 2019

Revised: September 11, 2019

Published online:

- [1] S. A. McDonald, G. Konstantatos, S. Zhang, P. W. Cyr, E. J. D. Klem, L. Levina, E. H. Sargent, *Nat. Mater.* **2005**, *4*, 138.
- [2] S. Coe-Sullivan, J. S. Steckel, W. K. Woo, M. G. Bawendi, V. Bulović, *Adv. Funct. Mater.* **2005**, *15*, 1117.
- [3] J. M. Caruge, J. E. Halpert, V. Wood, V. Bulović, M. G. Bawendi, *Nat. Photonics* **2008**, *2*, 247.
- [4] I. J. Kramer, E. H. Sargent, *Chem. Rev.* **2014**, *114*, 863.
- [5] M. Liu, O. Voznyy, R. Sabatini, F. P. García De Arquer, R. Munir, A. H. Balawi, X. Lan, F. Fan, G. Walters, A. R. Kirmani, S. Hoogland, F. Laquai, A. Amassian, E. H. Sargent, *Nat. Mater.* **2017**, *16*, 258.
- [6] C. H. M. Chuang, P. R. Brown, V. Bulović, M. G. Bawendi, *Nat. Mater.* **2014**, *13*, 796.
- [7] A. J. Labelle, S. M. Thon, S. Masala, M. M. Adachi, H. Dong, M. Farahani, A. H. Ip, A. Fratilocchi, E. H. Sargent, *Nano Lett.* **2015**, *15*, 1101.
- [8] R. A. Taylor, K. Ramasamy, *SPR Nanosci.* **2017**, *4*, 142.
- [9] M. Graetzel, R. A. J. Janssen, D. B. Mitzi, E. H. Sargent, *Nature* **2012**, *488*, 304.
- [10] S. Pradhan, A. Stavrinadis, S. Gupta, S. Christodoulou, G. Konstantatos, *ACS Energy Lett.* **2017**, *2*, 1444.
- [11] C. H. M. Chuang, A. Maurano, R. E. Brandt, G. W. Hwang, J. Jean, T. Buonassisi, V. Bulović, M. G. Bawendi, *Nano Lett.* **2015**, *15*, 3286.
- [12] S. Pradhan, A. Stavrinadis, S. Gupta, Y. Bi, F. Di Stasio, G. Konstantatos, *Small* **2017**, *13*, 1700598.
- [13] D. Kim, D. H. Kim, J. H. Lee, J. C. Grossman, *Phys. Rev. Lett.* **2013**, *110*, 196802.
- [14] D. K. Ko, A. Maurano, S. K. Suh, D. Kim, G. W. Hwang, J. C. Grossman, V. Bulović, M. G. Bawendi, *ACS Nano* **2016**, *10*, 3382.
- [15] G. W. Hwang, D. Kim, J. M. Cordero, M. W. B. Wilson, C. H. M. Chuang, J. C. Grossman, M. G. Bawendi, *Adv. Mater.* **2015**, *27*, 4481.
- [16] J. W. Jo, Y. Kim, J. Choi, F. P. G. de Arquer, G. Walters, B. Sun, O. Ouellette, J. Kim, A. H. Proppe, R. Quintero-Bermudez, J. Fan, J. Xu, C. S. Tan, O. Voznyy, E. H. Sargent, *Adv. Mater.* **2017**, *29*, 1.
- [17] D. Zhitomirsky, I. J. Kramer, A. J. Labelle, A. Fischer, R. Debnath, J. Pan, O. M. Bakr, E. H. Sargent, *Nano Lett.* **2012**, *12*, 1007.
- [18] Y. Liu, D. Kim, O. P. Morris, D. Zhitomirsky, J. C. Grossman, *ACS Nano* **2018**, *12*, 2838.
- [19] O. Voznyy, L. Levina, F. Fan, G. Walters, J. Z. Fan, A. Kiani, A. H. Ip, S. M. Thon, A. H. Proppe, M. Liu, E. H. Sargent, *Nano Lett.* **2017**, *17*, 7191.
- [20] J. Gao, C. L. Perkins, J. M. Luther, M. C. Hanna, H. Y. Chen, O. E. Semonin, A. J. Nozik, R. J. Ellingson, M. C. Beard, *Nano Lett.* **2011**, *11*, 3263.
- [21] P. R. Brown, R. R. Lunt, N. Zhao, T. P. Osedach, D. D. Wanger, L. Y. Chang, M. G. Bawendi, V. Bulović, *Nano Lett.* **2011**, *11*, 2955.
- [22] P. R. Brown, D. Kim, R. R. Lunt, N. Zhao, M. G. Bawendi, J. C. Grossman, V. Bulović, *ACS Nano* **2014**, *8*, 5863.

- 1 [23] H. Ishii, H. Oji, E. Ito, N. Hayashi, D. Yoshimura, K. Seki, *J. Lumin.* **2000**, *87*, 61. 1
- 2 2000, 87, 61. 2
- 3 [24] M. Grobosch, M. Knupfer, *Org. Electron.* **2007**, *8*, 625. 3
- 4 [25] K. Antoine, K. Norbert, G. Weiying, *J. Polym. Sci., Part B: Polym.* 4
- 5 *Phys.* **2003**, *41*, 2529. 5
- 6 [26] E. J. D. Klem, H. Shukla, S. Hinds, D. D. MacNeil, L. Levina, 6
- 7 E. H. Sargent, *Appl. Phys. Lett.* **2008**, *92*, 1. 7
- 8 [27] M. Vasilopoulou, A. Soultati, P. Argitis, T. Stergiopoulos, 8
- 9 D. Davazoglou, *J. Phys. Chem. Lett.* **2014**, *5*, 1871. 9
- 10 [28] L. S. Liao, W. K. Slusarek, T. K. Hatwar, M. L. Ricks, D. L. Comfort, 10
- Q9 11 [29] M. P. Patankar, K. Joshi, K. L. Narasimhan, arXiv:1312.0223. 11
- 12 [30] Y. Wang, Q. Liang, J. Huang, D. Ma, Y. Jiao, *RSC Adv.* **2017**, *7*, 12
- 13 28494. 13
- 14 [31] A. Opitz, M. Bronner, W. Brütting, *J. Phys.: Conf. Ser.* **2008**, *100*, 14
- 15 082043. 15
- Q10 16 [32] K. Tokunaga, *Hydrogenation of Fullerene C60: Material Design of* 16
- 17 *Organic Semiconductors by Computation*, IntechOpen, London **2012**. 17
- Q11 18 [33] T. Zhuang, X. F. Wang, T. Sano, Z. Hong, G. Li, Y. Yang, J. Kido, 18
- 19 *Appl. Phys. Lett.* **2014**, *105*, 093301. 19
- 20 [34] Q. Zhang, B. Kan, F. Liu, G. Long, X. Wan, X. Chen, Y. Zuo, W. Ni, 20
- 21 H. Zhang, M. Li, Z. Hu, F. Huang, Y. Cao, Z. Liang, M. Zhang, 21
- 22 T. P. Russell, Y. Chen, *Nat. Photonics* **2014**, *9*, 35. 22
- Q12 23 [35] M. Stollerfoht, S. Shoaee, A. Armin, H. Jin, I. Kassal, W. Jiang, 23
- 24 P. Burn, P. Meredith, *Adv. Energy Mater.* **2017**, *7*, 1601379. 24
- Q13 25 [36] T. D. Anthopoulos, D. M. De Leeuw, E. Cantatore, P. Van't Hof, 25
- 26 J. Alma, J. C. Hummelen, *J. Appl. Phys.* **2005**, *98*, 054503. 26
- 27 [37] B. Ebenhoch, S. A. J. Thomson, K. Genevičius, G. Juška, 27
- 28 I. D. W. Samuel, *Org. Electron.* **2015**, *22*, 62. 28
- 29 [38] K. Cnops, B. P. Rand, D. Cheyons, B. Verreert, M. A. Empl, 29
- 30 P. Heremans, *Nat. Commun.* **2014**, *5*, 1. 30
- 31 [39] C. Xiang, W. Koo, F. So, H. Sasabe, J. Kido, *Light: Sci. Appl.* **2013**, 31
- 32 2, 1. 32
- 33 [40] M. Nikolka, I. Nasrallah, B. Rose, M. K. Ravva, K. Broch, 33
- 34 A. Sadhanala, D. Harkin, J. Charmet, H. Hurhangee, A. Brown, 34
- 35 S. Illig, P. Too, J. Jongman, I. McCulloch, J. L. Bredas, 35
- Q14 36 H. Sirringhaus, *Nat. Mater.* **2017**, *16*, 356. 36
- 37 [41] S. Ambrozevich, M. Van Der Auweraer, D. Dirin, M. Parshin, 37
- 38 R. Vasil'Ev, A. Vitukhnovsky, *J. Russ. Laser Res.* **2008**, *29*, 526. 38
- Q15 39 [42] H. H. Fong, S. K. So, *J. Appl. Phys.* **2006**, *100*, 094502. 39
- 40 [43] T. D. Hoanh, Y. H. Im, D.-E. Kim, Y.-S. Kwon, B.-J. Lee, *J. Nano-* 40
- Q16 41 *mater.* **2012**, *2012*, 7. 41
- 42 [44] N. Mendil, M. Daoudi, Z. Berkai, A. Belghachi, *J. Phys.: Conf. Ser.* 42
- 43 **2014**, *647*, 012057. 43
- 44 [45] C. Kulshreshtha, G. W. Kim, R. Lampande, D. H. Huh, M. Chae, 44
- 45 J. H. Kwon, *J. Mater. Chem. A* **2013**, *1*, 4077. 45
- 46 [46] H. Kim, K. G. Lim, T. W. Lee, *Energy Environ. Sci.* **2016**, *9*, 12. 46
- 47 [47] J. Hou, X. Guo, in *Organic Solar Cells: Materials Device Physics* (Ed: 47
- 48 W. C. H. Choy), Springer London, London, **2013**, pp. 17–42. 48
- 49 [48] S. Cho, J. H. Seo, S. H. Park, S. Beaupré, M. Leclerc, A. J. Heeger, 49
- 50 *Adv. Mater.* **2010**, *22*, 1253. 50
- 51 51
- 52 52
- 53 53
- 54 54
- 55 55
- 56 56
- 57 57
- 58 58
- 59 59
- [49] S. Cheylan, J. Puigdollers, H. J. Bolink, E. Coronado, C. Voz, 1
- R. Alcubilla, G. Badenes, *J. Appl. Phys.* **2008**, *103*, 10. 2
- [50] M. Morana, M. Wegscheider, A. Bonanni, N. Kopidakis, S. Shaheen, 3
- M. Scharber, Z. Zhu, D. Waller, R. Gaudiana, C. Brabec, *Adv. Funct.* 4
- Mater.* **2008**, *18*, 1757. 5
- [51] M. D. Ho, D. Kim, N. Kim, S. M. Cho, H. Chae, *ACS Appl. Mater.* 6
- Interfaces* **2013**, *5*, 12369. 7
- [52] A. W. Hains, T. J. Marks, *Appl. Phys. Lett.* **2008**, *92*, 023504. 7
- [53] M. Geoghegan, G. Hadziioannou, *Polymer Electronics* **2013**. 8
- [54] C. A. Amorim, M. R. Cavallari, G. Santos, F. J. Fonseca, 9
- A. M. Andrade, S. Mergulhão, *J. Non-Cryst. Solids* **2012**, *358*, 484. 10
- [55] F. Huang, Y. Peng, K. Xu, W. Lv, S. Xu, Y. Wang, Y. Tang, Y. Wei, 11
- Y. Yang, G. Liu, *J. Phys. D: Appl. Phys.* **2017**, *50*, <http://doi.org/10.1088/1361-6463/aa6bdc>. 12
- [56] F. Zhao, X. Luo, J. Liu, L. Du, W. L. Lv, L. Sun, Y. Li, Y. Wang, Y. Peng, 13
- J. Mater. Chem. C* **2015**, *4*, 815. 14
- [57] M. A. Loi, E. D. A. Como, F. Dinelli, M. Murgia, R. Zamboni, 15
- F. Biscarini, M. Muccini, *Nat. Mater.* **2005**, *4*, 81. 16
- [58] A. V. Patil, W. H. Lee, K. Kim, H. Park, I. N. Kang, S. H. Lee, *Polym.* 17
- Chem.* **2011**, *2*, 2907. 18
- [59] T.-W. Lee, K.-G. Lim, D.-H. Kim, *Electron. Mater. Lett.* **2010**, *6*, 41. 19
- [60] K. Yang, Y. Wang, A. Jain, L. Samulson, J. Kumar, *J. Macromol. Sci.,* 20
- Part A: Pure Appl. Chem.* **2007**, *44*, 1261. 21
- [61] H. Wei, L. Scudiero, H. Eilers, *Appl. Surf. Sci.* **2009**, *255*, 8593. 22
- [62] F. Yang, C. Li, J. Zhang, G. Feng, Z. Wei, W. Li, *Org. Electron.* **2016**, 23
- 37*, 366. 24
- [63] Y. Liu, Q. Chen, H. S. Duan, H. Zhou, Y. Yang, H. Chen, S. Luo, 25
- T. Bin Song, L. Dou, Z. Hong, Y. Yang, *J. Mater. Chem. A* **2015**, *3*, 26
11940. 27
- [64] F. Ullah, H. Chen, C. Z. Li, *Chinese Chem. Lett.* **2017**, *28*, 503. 27
- [65] D. H. Kim, K. G. Lim, J. H. Park, T. W. Lee, *ChemSusChem* **2012**, *5*, 28
2053. 29
- [66] A. Lenz, H. Kariis, A. Pohl, P. Persson, L. Ojamäe, *Chem. Phys.* 30
- 2011**, *384*, 44. 31
- [67] Y. Kanai, J. C. Grossman, *Nano Lett.* **2007**, *7*, 1967. 32
- [68] K. Anil, W. Milne, J. Jang, *Sol. Energy Mater. Sol. Cells* **2015**, *132*, 33
623. 34
- [69] M. T. Greiner, M. G. Helander, W. M. Tang, Z. Bin Wang, J. Qiu, 35
- Z. H. Lu, *Nat. Mater.* **2012**, *11*, 76. 36
- [70] M. Jørgensen, K. Norrman, F. C. Krebs, *Sol. Energy Mater. Sol. Cells* 37
- 2008**, *92*, 686. 38
- [71] K. Norrman, M. V. Madsen, S. A. Gevorgyan, F. C. Krebs, 39
- V. Frederiksborg, D. Roskilde, **2010**, 16883. 40
- [72] J. F. G. Kresse, *Phys. Rev. B - Condens. Matter Mater. Phys.* **1996**, *54*, 40
169. 41
- [73] D. G. Kresse, *Joubert, Phys. Rev. B - Condens. Matter Mater. Phys.* 42
- 1999**, *59*, 1758. 43
- [74] B. Hammer, L. B. Hansen, J. K. Nørskov, *Phys. Rev. B - Condens.* 44
- Matter Mater. Phys.* **1999**, *59*, 7413. 45
- [75] Y. Cheng, E. S. Arinze, N. Palmquist, S. M. Thon, *Nanophotonics* 46
- 2016**, *5*, 31. 47
- 48
- 49
- 50
- 51
- 52
- 53
- 54
- 55
- 56
- 57
- 58
- 59

**Reprint Order Form 2019**  
**- please return with your proofs -**

**Manuscript No.** \_\_\_\_\_

Please send me and bill me for

no. of reprints via  airmail (+ 25 Euro)  
 surface mail

**high-resolution PDF file** (330 Euro).

My e-mail address:

\_\_\_\_\_

Please note: It is not permitted to present the PDF file on the internet or on company homepages

★**Special Offer**★ If you order 200 or more reprints you will get a PDF file for half price.

**Information regarding VAT**

Please note that from German sales tax point of view, the charge for **Reprints, Issues or Posters** is considered as "supply of goods" and therefore, in general, such delivery is a subject to German sales tax. However, this regulation has no impact on customers located outside of the European Union. Deliveries to customers outside the Community are automatically tax-exempt. Deliveries within the Community to institutional customers outside of Germany are exempted from the German tax (VAT) only if the customer provides the supplier with his/her VAT number. The VAT number (value added tax identification number) is a tax registration number used in the countries of the European Union to identify corporate entities doing business there. It starts with a country code (e.g. FR for France, GB for Great Britain) and follows by numbers.

**Cover Posters**

Posters are available of all the published covers and frontispieces in two sizes

DIN A2 42 x 60 cm/ 17 x 24in (one copy: **39 Euro**)

DIN A1 60 x 84 cm/ 24 x 33in (one copy: **49 Euro**)

Postage for shipping posters overseas by airmail:  
**+ 25 Euro**

Postage for shipping posters within Europe by surface mail:  
**+ 15 Euro**

**Mail reprints / cover posters to:**

\_\_\_\_\_

\_\_\_\_\_

\_\_\_\_\_

\_\_\_\_\_

**Invoice address:**

\_\_\_\_\_

\_\_\_\_\_

\_\_\_\_\_

\_\_\_\_\_

\_\_\_\_\_  
**Date, Signature** **Stamp**

**VAT no.:** \_\_\_\_\_  
(institutes / companies in EU countries only)

**Purchase Order No.:** \_\_\_\_\_

**Credit Card Payment**

**VISA, MasterCard, AMERICAN EXPRESS**

Please use the Credit Card Token Generator located at the website below to create a token for secure payment. The token will be used instead of your credit card number.

**Credit Card Token Generator:**

[https://www.wiley-vch.de/editorial\\_production/index.php](https://www.wiley-vch.de/editorial_production/index.php)

Please transfer your token number to the space below.

**Credit Card Token Number:**

--	--	--	--	--	--	--	--	--	--	--	--	--	--	--	--	--	--	--	--

**Price list for reprints** (The prices include mailing and handling charges. All Wiley-VCH prices are exclusive of VAT)

No. of pages	Price (in Euro) for orders of					
	50 copies	100 copies	150 copies	200 copies	300 copies	500 copies
1-4	345	395	425	445	548	752
5-8	490	573	608	636	784	1077
9-12	640	739	786	824	1016	1396
13-16	780	900	958	1004	1237	1701
17-20	930	1070	1138	1196	1489	2022
for every additional 4 pages	147	169	175	188	231	315

★ **Special Offer** ★ If you order 200 or more reprints you will get a PDF file for half price.